

# Tversky as a Loss Function for Highly Unbalanced Image Segmentation using 3D Fully Convolutional Deep Networks

Seyed Raein Hashemi<sup>1,2</sup>, Seyed Sadegh Mohseni Salehi<sup>1,3</sup>, *Student Member, IEEE*,  
 Deniz Erdogmus<sup>3</sup>, *Senior Member, IEEE*, Sanjay P. Prabhu<sup>1</sup>,  
 Simon K. Warfield<sup>1</sup>, *Senior Member, IEEE*, and Ali Gholipour<sup>1</sup>, *Senior Member, IEEE*

<sup>1</sup>Computational Radiology Laboratory, Boston Children's Hospital, and Harvard Medical School, Boston MA 02115

<sup>2</sup>Computer and Information Science Department, Northeastern University, Boston, MA, 02115

<sup>3</sup>Electrical and Computer Engineering Department, Northeastern University, Boston, MA, 02115

**Fully convolutional deep neural networks have been asserted to be fast and precise frameworks with great potential in image segmentation. One of the major challenges in utilizing such networks is data imbalance, which is especially restraining in medical imaging applications such as lesion segmentation where lesion class voxels are often much less than non-lesion voxels. A trained network with unbalanced data may make predictions toward high precision and low recall (sensitivity), being severely biased towards the non-lesion class which is particularly undesired in medical applications where false negatives are actually more important than false positives. Several methods have been proposed to deal with this problem including balanced sampling, two step training, sample re-weighting, and similarity loss functions. In this paper, we propose a generalized loss function based on the Tversky index to mitigate the issue of data imbalance and achieve much better trade-off between precision and recall in training 3D fully convolutional deep neural networks. Moreover, we extend our preliminary work on using Tversky loss function for U-net to a patch-wise 3D densely connected network, where we use overlapping image patches for intrinsic and extrinsic data augmentation. To this end, we propose a patch prediction fusion strategy based on B-spline weighted soft voting to take into account the uncertainty of prediction in patch borders.**

The lesion segmentation results obtained from our patch-wise 3D densely connected network are superior to the recently reported results in the literature on multiple sclerosis lesion segmentation on magnetic resonance imaging dataset, namely MSSEG 2016, in which we obtained average Dice coefficient of 69.8%. Significant improvement in  $F_1$  and  $F_2$  scores and the area under the precision-recall curve was achieved in test using the Tversky loss layer and via our 3D patch prediction fusion method. Based on these results we suggest Tversky loss function as a generalization of the Dice similarity coefficient and  $F_\beta$  scores to effectively train deep neural networks.

**Index Terms**—Lesion segmentation, Tversky loss function, Convolutional neural network, DenseNet, Patch prediction fusion.

Copyright (c) 2018 IEEE. Personal use of this material is permitted. However, permission to use this material for any other purposes must be obtained from the IEEE by sending a request to [pubs-permissions@ieee.org](mailto:pubs-permissions@ieee.org).

Manuscript received March 30, 2018. This study was supported in part by the National Institutes of Health grants R01 NS079788 and R01 EB018988; and in part by a Technological Innovations in Neuroscience Award from the McKnight Foundation. The content of this work is solely the responsibility of the authors and does not necessarily represent the official views of the NIH or the McKnight Foundation. Corresponding author: S.R.Hashemi (email: hashemi.s@husky.neu.edu).

## I. INTRODUCTION

CONVOLUTIONAL neural networks have shown promising results in a wide range of applications including image segmentation. Recent medical image segmentation literature shows significant progress towards automatic segmentation of brain lesions [1], [2], tumors [3], [4], [5], and neuroanatomy [6], [7], [8] using 2D networks [3], [6], [9], and more recently using 3D network architectures [8], [2], in particular fully convolutional networks (FCNs) [9], [10], [11].

Multiple sclerosis (MS) is the most common disabling neurologic autoimmune disease resulting from recurrent attacks of inflammation in the central nervous system [12], [13]. Across the extensive literature for automated MS lesion segmentation, there are methods which try to alleviate the data imbalance issue by equal selection of training samples from each class [3], [14], whereas others propose using more persistent loss functions [1], [11], [15], both of which we combine together as a rigorous solution. In this work, we investigate and compare the generality and performance of our proposed loss function based on the Tversky index [16] with the Dice similarity loss function recently proposed for segmentation using FCNs [11], especially with significantly unbalanced data.

In addition, we further diminish the problem of data imbalance by using patches that lead to relatively higher ratio of lesion versus non-lesion. Overlapping patches provide intrinsic data augmentation, make a better balance in data for training, and make the network adaptable for any size inputs with efficient memory usage in both test and training. We propose a patch prediction fusion strategy to take into account the prediction uncertainty in patch borders. In what follows, we review the state-of-the-art in lesion segmentation and the related work that motivated this study. Then we show two network architectures with our proposed loss function that generate accurate lesion segmentation compared to the literature according to several performance metrics.

## II. RELATED WORK

Many novel and genuine algorithms, methods and models have been continuously developed and improved over the past years on lesion segmentation. As the number of these methods grew, so did the desire for higher precision and

more general solutions. In spite of the fact that there are lots of fully automated segmentation algorithms, the accuracy of these methods are not yet in an acceptable range, highlighting the difficulty of the problem. Therefore, lesion segmentation remains an active and important area of research.

The state-of-the-art lesion segmentation methods mostly use aggregations of skull stripping, bias correction, image registration, atlases, intensity feature information, data augmentation and the use of a prior or mask in training. The most recently proposed deep learning techniques for lesion segmentation include cascaded convolutional neural networks [17], [18], deep convolutional encoder networks [1], [19], and independent image modality convolution pipelines [20]. There has also been other more classic supervised methods such as decision random forests [21], [22], non-local means [23], [24], and combined inference from patient and healthy populations [25]. One of the most recent techniques for the application of lesion segmentation, proposes the use of generalized dice overlap as a loss function [26] which assigns weights to different segmentation labels based on their quantity and volume in the training data. The other recent technique merges the two popular architectures of Unet and DenseNet while forming a hybrid structure [27] for liver and tumor segmentation.

In this study, we propose the Tversky loss function to train deep fully convolutional neural networks based on two architectures: the Unet due to its fast speed attribute [28] and DenseNet because of its deep infrastructure [29], both in a 3D manner. A preliminary report of this work in using Tversky as a loss function for 3D U-net was presented at MLMI2017 [30]. To the best of our knowledge this is the first work proposing a loss function for precision and recall adjustments, applied on 3D deep networks with highly unbalanced data. Within our approach, we investigate the effects of the Tversky loss function on whole-size as well as patch-size images with two different deep networks. In addition, we incorporate a soft weighted voting method, calculating weighted average of probabilities predicted by many augmented overlapping patches in an image. Our results show that this significantly improved lesion segmentation accuracy. Based on our experimental results, we strongly recommend the use of precision-recall balancing properties of the Tversky index as a novel loss function for both balanced and unbalanced data.

### III. METHOD

#### A. Network Architecture

We designed and evaluated two fully convolutional neural networks with two different network architectures: 1) a 3D fully convolutional network [31], [32] based on the U-net architecture [15], and 2) a 3D densely connected network [29] based on the Dense-Net architecture [33]. To this end, we develop a 3D U-net and a 3D patch-wise Dense-Net while introducing a Tversky loss layer [30] based on the Tversky index [16]. The details of the network architectures are described next and we follow with the loss function formulation, and our proposed 3D patch prediction fusion method for the patch-wise network.

#### 1) 3D Unet

We propose a 3D U-net based on Auto-Net [9] and introduce a new loss layer [30] based on the Tversky index. This U-net style architecture, which has been designed to work with very small number of training images, is shown in Figure 1. It consists of a contracting path (to the right) and an expanding path (to the left). To learn and use local information, high-resolution 3D features in the contracting path are concatenated with upsampled versions of global low-resolution 3D features in the expanding path. Through this concatenation the network learns to use both high-resolution local features and low-resolution global features.

The contracting path contains padded  $3 \times 3 \times 3$  convolutions followed by ReLU non-linear layers. A  $2 \times 2 \times 2$  max pooling operation with stride 2 is applied after every two convolutional layers. After each downsampling by the max pooling layers, the number of features is doubled. In the expanding path, a  $2 \times 2 \times 2$  transposed convolution operation is applied after every two convolutional layers, and the resulting feature map is concatenated to the corresponding feature map from the contracting path. At the final layer a  $1 \times 1 \times 1$  convolution with softmax output is used to reach the feature map with a depth equal to the number of classes (lesion or non-lesion).

#### 2) 3D patch-wise Dense-Net

We propose a 3D patch-wise Dense-Net based on 3D DenseSeg [33] with overlapping patches, a new loss layer based on the Tversky index, and a patch prediction fusion strategy. Figure 2 shows the schematic architecture of the 3D patch-wise Dense-Net. This Dense-Net style architecture consists of three initial  $3 \times 3 \times 3$  convolutional layers followed by five dense blocks with a growth rate of 12. Growth rate refers to the increase amount in the number of feature maps after each layer in a dense block. In each dense block there are four  $3 \times 3 \times 3$  convolutional layers preceding with  $1 \times 1 \times 1$  convolutional layers referred to as bottlenecks [29], which have the purpose of reducing the number of input feature maps. Skip connections are made between all layers of each dense block. Aside from the last dense block, others are followed by a  $1 \times 1 \times 1$  convolutional layer and a max pooling layer which are named transition blocks. Down sampling of stride two occurs in each transition block to reduce the feature map dimensionality for computational efficiency. Each of the convolutional layers is followed by batch normalization and ReLU activation layers. Dropout rate of 0.2 is only applied after  $3 \times 3 \times 3$  convolutional layers within dense blocks. At the final layer a  $1 \times 1 \times 1$  convolution with sigmoid output is used to reach the feature map with depth of one (lesion or non-lesion class).

Prior to proceeding to the main classifier, results of all dense blocks are upsampled using deconvolutional layers, using transpose matrices of convolutions. Afterwards, the results are concatenated and passed through the main classifier to calculate the probability map of the input patch. In the proposed architecture, fully convolutional layers are used instead of fully connected layers [34] to achieve much faster testing time. This architecture segments a 3D image patch of size  $64 \times 64 \times 64$ . Therefore, to segment any size input image,

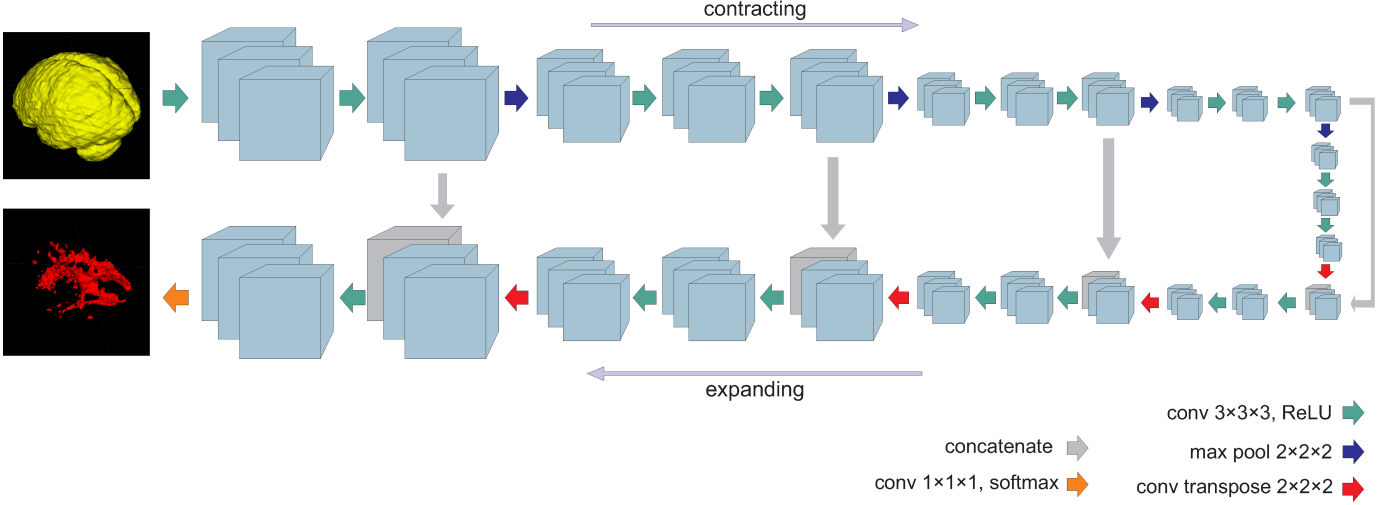


Figure 1. The 3D U-net style architecture with full-size images as inputs and skip connections between a contracting path and an expanding path.

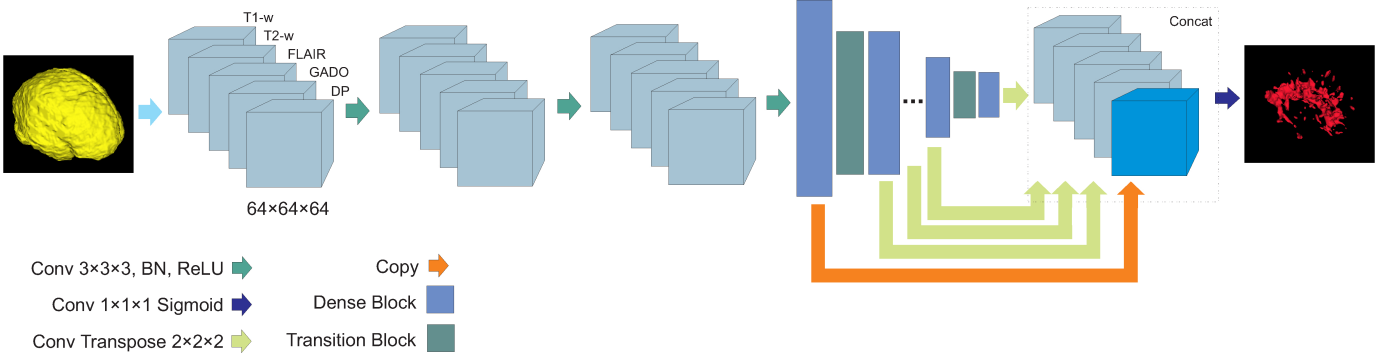


Figure 2. The 3D patch-wise Dense-Net style architecture with  $64 \times 64 \times 64$  five channel input patches, consisting of five dense blocks and four convolutional layers with bottlenecks within each block. Overlapping patches of a full size image are used as inputs to this network for training and testing.

overlapping patches of size  $64 \times 64 \times 64$  extracted from the image are used as input to the network. These patches are augmented and their predictions are fused to provide final segmentation of a full-size input image. The loss layer, patch augmentation and patch prediction fusion, and the details of training are discussed in the sections that follow.

### B. Tversky loss layer

The output layer in the networks consists of  $c$  planes, one per class ( $c = 2$  in lesion segmentation). We applied softmax along each voxel to form the loss. Let  $P$  and  $G$  be the set of predicted and ground truth binary labels, respectively. The Dice similarity coefficient  $D$  between  $P$  and  $G$  is defined as:

$$D(P, G) = \frac{2|PG|}{|P| + |G|} \quad (1)$$

A loss function based on the Dice similarity coefficient has been proposed as an alternative to cross entropy to improve training 3D U-net [11]; however  $D$ , as the harmonic mean of precision and recall, weighs false positives (FPs) and false negatives (FNs) equally. To make a better adjustment of the weights of FPs and FNs (and a better balance between precision and recall) in training fully convolutional networks

for highly unbalanced data, where detecting small lesions is crucial, we propose a loss layer based on the Tversky index [16]. The Tversky index is defined as:

$$S(P, G; \alpha, \beta) = \frac{|PG|}{|PG| + \alpha|P \setminus G| + \beta|G \setminus P|} \quad (2)$$

where  $P \setminus G$  is the relative complement of  $G$  on  $P$ , and  $\alpha$  and  $\beta$  control the magnitude of penalties for FPs and FNs, respectively.

To define the Tversky loss function we use the following formulation:

$$T(\alpha, \beta) = \frac{\sum_{i=1}^N p_{0i}g_{0i}}{\sum_{i=1}^N p_{0i}g_{0i} + \alpha \sum_{i=1}^N p_{0i}g_{1i} + \beta \sum_{i=1}^N p_{1i}g_{0i}} \quad (3)$$

where in the output of the softmax layer, the  $p_{0i}$  is the probability of voxel  $i$  be a lesion and  $p_{1i}$  is the probability of voxel  $i$  be a non-lesion. Also, the ground truth training label  $g_{0i}$  is 1 for a lesion voxel and 0 for a non-lesion voxel and vice versa for the  $g_{1i}$ . The gradient of the loss in (3) with respect to  $p_{0i}$  and  $p_{1i}$  can be calculated as:

$$\frac{\partial T}{\partial p_{0i}} = 2 \left( \frac{g_{0j} (\sum_{i=1}^N p_{0i} g_{0i} + \alpha \sum_{i=1}^N p_{0i} g_{1i} + \beta \sum_{i=1}^N p_{1i} g_{0i})}{(\sum_{i=1}^N p_{0i} g_{0i} + \alpha \sum_{i=1}^N p_{0i} g_{1i} + \beta \sum_{i=1}^N p_{1i} g_{0i})^2} \right) \quad (4)$$

$$\frac{\partial T}{\partial p_{1i}} = - \frac{\beta g_{1j} \sum_{i=1}^N p_{0i} g_{0i}}{(\sum_{i=1}^N p_{0i} g_{0i} + \alpha \sum_{i=1}^N p_{0i} g_{1i} + \beta \sum_{i=1}^N p_{1i} g_{0i})^2} \quad (5)$$

Using this formulation we do not need to balance the weights for training. Also by adjusting the hyperparameters  $\alpha$  and  $\beta$  we can control the trade-off between FPs and FNs. It is noteworthy that in the case of  $\alpha = \beta = 0.5$  the Tversky index simplifies to be the same as the Dice similarity coefficient, which is also equal to the  $F_1$  score. With  $\alpha = \beta = 1$ , (2) results in the Tanimoto coefficient, and setting  $\alpha + \beta = 1$  leads to the set of  $F_\beta$  scores. Larger  $\beta$ s weigh recall higher than precision (by placing more emphasis on false negatives). We hypothesize that using higher  $\beta$ s in our generalized loss function in training helps us shift the emphasis to decrease FNs and boost recall, hence achieve better performance in terms the precision-recall trade-off.

### C. 3D Patch Prediction Fusion Method

To use our 3D patch-wise Dense-Net architecture to segment a full-size input image (of any size), overlapping patches (of size  $64 \times 64 \times 64$ ) are taken from the image and fed into the network. In both training and testing, patches are augmented, fed into the network, and their predictions are fused in a procedure that is described in this section.

The amount of intersection area (overlap) between patches is adjustable. If we were to use 75% overlaps, the prediction time would be roughly an hour per 3D image. However, to keep the prediction time close to 5 minutes per image, we used 50% overlaps (stride of 1/2 of the patch size) on patch windows. Therefore, given the input image sizes of  $128 \times 224 \times 256$ , the algorithm produces  $5 \times 8 \times 9$  patches per augmentation. There are four augmentations, the original image, and the three 180 degree rotations for each plane. Consequently, our model performs 1,440 patch predictions per 3D image (from the MSSEG2016) and 32 predictions per voxel.

The predictions from overlapping patches are fused to form the segmentation of the full-size image. In case of no overlap and no patch augmentation, each voxel on the original image has one predicted value, therefore predictions from tiled patches can just be tiled to produce the original image segmentation. However, this does not lead to the best results due to the lack of augmentation in test and training and also because patch predictions are less accurate in the patch borders due to incomplete image features in patch borders. This is shown in Figure 3 where lesions in the border of patches are not correctly segmented in the tiling method where no overlap between patches was used. In the second column, where patches with 50% overlap were used, each voxel received multiple predictions from overlapping patches.

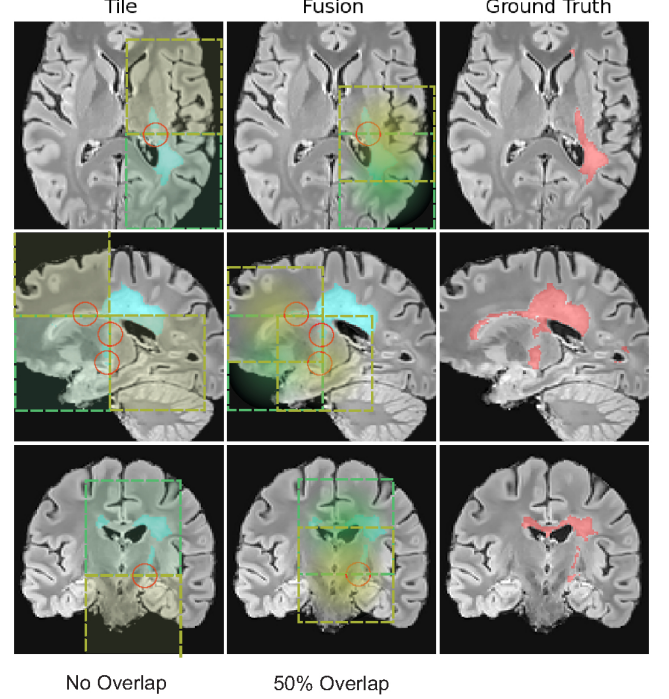


Figure 3. Patch selection of the fusion method compared to the patch tiling method. The predictions are based on the DenseNet model with  $\beta = 0.7$ . Voxels near patch borders get relatively lower accuracy predictions when a tiling approach is used, while for the fusion approach voxels near the border of one patch will be at the center of another patch resulting in a higher accuracy. The differences of predictions are shown with red circles.

To take into account the relative uncertainty of predictions near patch borders, we use a weighted soft voting approach to fuse patch predictions as opposed to the conventional voting (averaging) method, e.g. [35]. To this end, we calculate the relative weights of soft predictions using a second-order spline function at each patch center. This allows fusion of predictions from all overlapping and augmented patches while giving lower weights to predictions that are made by patches on their borders. With 50% overlap, voxels near the borders of one patch are near the center of another patch as is seen in Figure 3. In our experiments we compared different scenarios, in particular compared our proposed spline patch prediction fusion with uniform patch prediction fusion and patch tiling.

### D. Training

We trained our two FCNs with Tversky loss layers to segment multiple sclerosis (MS) lesions [36], [17]. The details of the training processes of each network are described here.

#### 1) 3D Unet

Our 3D Unet was trained end-to-end. Cost minimization on 1000 epochs was performed using ADAM optimizer [37] with an initial learning rate of 0.0001 multiplied by 0.9 every 1000 steps. The training time for this network was approximately 4 hours on a workstation with Nvidia Geforce GTX1080 GPU.

#### 2) 3D patch-wise Dense-Net

Our 3D patch-wise Dense-Net was trained end-to-end. Cost minimization on 5000 epochs was performed using ADAM optimizer [37] with an initial learning rate of 0.0005 multiplied

by 0.95 every 500 steps with a step growth rate of 2 every 16,000 steps. For instance, the first growth happens at the 16,000th step, where the interval of 500 would be multiplied by two. The training time for this network was approximately 18 hours on a workstation with Nvidia Geforce GTX1080 GPU. The input patch size was chosen  $64 \times 64 \times 64$  as a balance between accuracy of extracted features (field of view) in each patch and limitations on the GPU memory. The selected size appeared to be both effective and practical.

Tversky (and similarly, Dice) loss function relies on true positive (TP) counts. The network would not be able to learn if the TP value is zero leading to a zero loss value. Therefore, only patches with a minimum of 10 lesion voxels were selected for training the patch-wise DenseNet architecture. Nevertheless, equal number of patches was selected from each image. Therefore, the FCNs trained equally with the training data, although they may have had a more diverse pool on images with more number of lesion voxels.

### E. Testing

In order to test the architectures properly, five-fold cross validation was used as the total number of subjects was very limited. Each fold contained 3 subjects each from 3 different centers. In order to test each fold we trained the networks each time from the beginning using the other 4 folds containing images of 12 subjects. After feeding forward the test subjects through the networks, voxels with computed probabilities of 0.5 or more were considered to belong to the lesion class and those with probabilities  $< 0.5$  were considered non-lesion.

## IV. EXPERIMENTS

### A. Datasets

We trained and evaluated our networks on the data set from MS lesion segmentation (MSSEG) challenge of the 2016 Medical Image Computing and Computer Assisted Intervention (MICCAI) conference. T1-weighted, T2-weighted FLAIR, Gadolinium-enhanced T1-weighted MRI, Proton Density (PD), and T2-weighted MRIs of 15 subjects were used as five channel inputs. Every group of five subjects were in different domains: 1) Philips Ingenia 3T, 2) Siemens Aera 1.5T and 3) Siemens Verio 3T. Images of different sizes were all rigidly registered to a reference image of size  $128 \times 224 \times 256$ . After registration, average lesion voxels per image was 15,500, with a maximum of 51,870 and a minimum of 647 voxels.

### B. Evaluation

To evaluate the performance of the networks and compare them against state-of-the-art in MS lesion segmentation, we report Dice similarity coefficient (DSC):  $DSC = \frac{2|P \cap G|}{|P| + |G|} = \frac{2TP}{2TP + FP + FN}$ , where  $P$  and  $G$  are the predicted and ground truth labels, respectively; and  $TP$ ,  $FP$ , and  $FN$  are the true positive, false positive, and false negative rates, respectively. We also calculate and report specificity,  $\frac{TN}{TN + FP}$ , and sensitivity,  $\frac{TP}{TP + FN}$ , and the  $F_2$  score as a measure that is commonly used in applications where recall is more important than precision (as compared to  $F_1$  or DSC):  $F_2 = \frac{5TP}{5TP + 4FN + FP}$ .

To critically evaluate the performance of the detection for the highly unbalanced (skewed) dataset, we use the Precision-Recall (PR) curve (as opposed to the receiver-operator characteristic, or ROC, curve) as well as the area under the PR curve (the APR score) [38], [39], [40]. For such skewed datasets, the PR curves and APR scores (on test data) are preferred figures of algorithm performance.

### C. Results

To evaluate the effect of Tversky loss function and compare it with Dice in lesion segmentation, we trained our FCNs with different  $\alpha$  and  $\beta$  values. The performance metrics are reported in Table I. The results show that 1) the balance between sensitivity and specificity was controlled by the parameters of the loss function; 2) according to all combined test measures, the best results were obtained from the FCNs trained with  $\beta = 0.7$ , which performed better than the FCNs trained with the Dice loss layer corresponding to  $\alpha = \beta = 0.5$ ; 3) the results obtained from 3D patch-wise DenseNet was much better than the results obtained by 3D U-net; and 4) our proposed spline fusion of patch predictions led to improved performance of the patch-wise DenseNet with tiling and uniform patch prediction fusion. Overall, the best results were obtained with the 3D patch-wise DenseNet with Tversky loss at  $\beta = 0.7$ , and spline-weighted soft voting fusion of patch predictions.

Figures 4 and 5 show the effect of different penalty magnitudes ( $\beta$ s) on segmenting a subject with high density of lesions and a subject with very few lesions, respectively. The improvement by using the Tverskey loss function is specifically significant in cases with very small number of lesion voxels as we can see in Figure 5. Independent of the network architecture, training with the Dice loss function ( $\beta = 0.5$ ), resulted in a high number of false negatives as many lesions were missed. Note that a high value of  $\beta = 0.9$  also resulted in a drop in performance. As it can be seen in PR-Curves (Figure 7) and APR results in Table I for different architectures, the best results corresponding to a good trade-off between sensitivity and specificity was achieved using Tversky with  $\beta = 0.7$ . Although,  $\beta = 0.7$  slightly decreased specificity, it led to a significant improvement in sensitivity (Figure 6) and the APR,  $F_1$  and  $F_2$  scores (Table I).

## V. DISCUSSION

With our proposed 3D patch-wise DenseNet method we achieved improved precision-recall trade-off and a high average DSC of 69.8 which is better than the highest ranked techniques examined on the 2016 MSSEG challenge. The 1st ranked team [41] achieved an average DSC of 67, and the 4th ranked team [42] achieved an average DSC of 66.6. We achieved an improved performance by using a 3D patch-wise DenseNet architecture together with the Tversky loss function and our patch prediction fusion method.

Experimental results in MS lesion segmentation show that all performance evaluation metrics (on the test data) improved by using the Tversky loss function rather than using the Dice similarity coefficient in the loss layer. While the loss

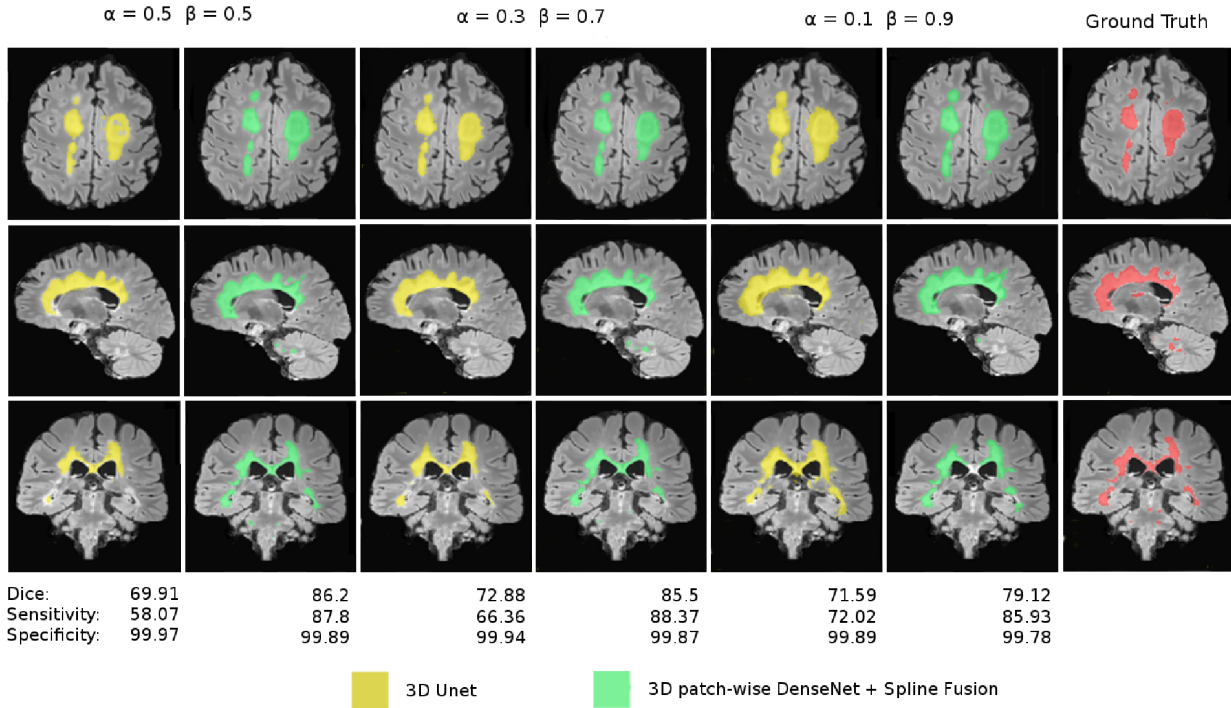


Figure 4. The effect of different penalties on FP and FN in the Tverskey loss function on a case with extremely high density of lesions. Axial, sagittal, and coronal sections of images have been shown and the Dice, sensitivity, and specificity values of each case are shown underneath the corresponding column. The best results were obtained at  $\beta = 0.7$  with our proposed 3D patch-wise DenseNet with spline patch prediction fusion.

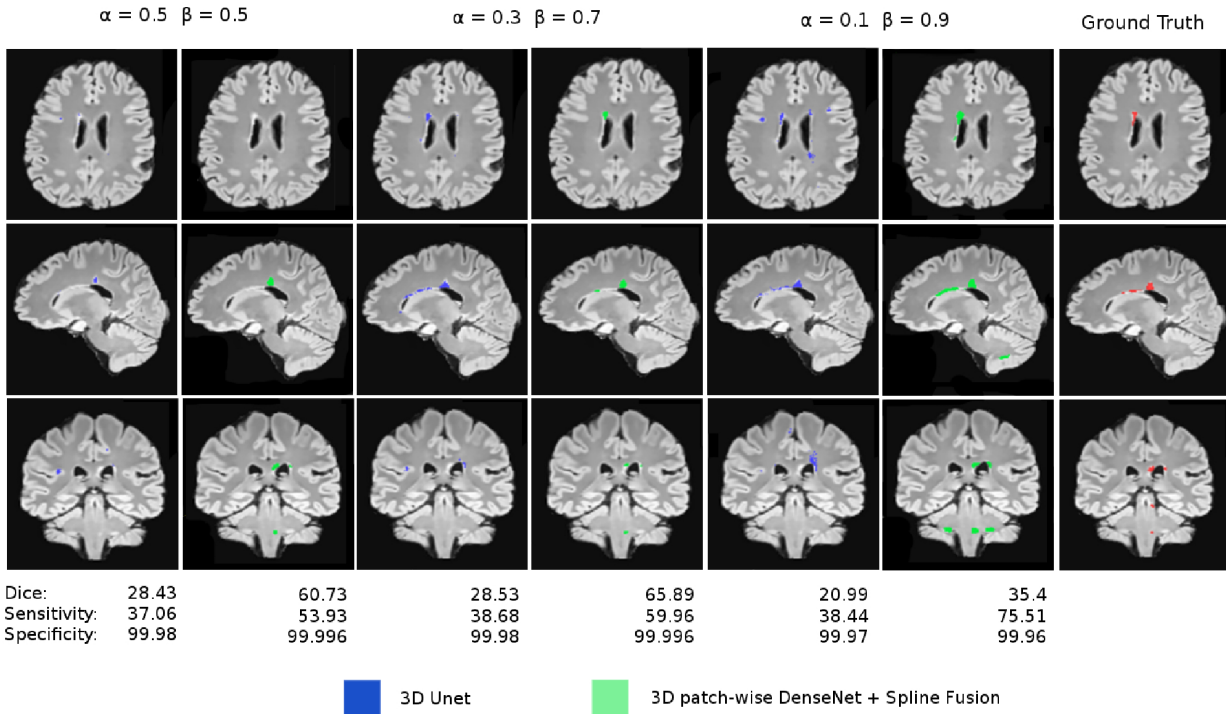


Figure 5. The effect of different penalties on FP and FN in the Tverskey loss function on a case with extremely low density of lesions. Axial, sagittal, and coronal sections of images have been shown and the Dice, sensitivity, and specificity values of each case are shown underneath the corresponding column. The best results were obtained at  $\beta = 0.7$  with our proposed 3D patch-wise DenseNet with spline patch prediction fusion.

Table I

PERFORMANCE METRICS (ON THE TEST SET) FOR DIFFERENT VALUES OF THE HYPERPARAMETERS  $\alpha$  AND  $\beta$  USED IN TRAINING THE 3D U-NET ON FULL-SIZE IMAGES, AND 3D PATCH-WISE DENSENET WITH DIFFERENT PATCH PREDICTION FUSION METHODS. THE BEST VALUES FOR EACH METRIC HAVE BEEN HIGHLIGHTED IN BOLD. AS EXPECTED, IT IS OBSERVED THAT HIGHER  $\beta$  LED TO HIGHER SENSITIVITY (RECALL) AND LOWER SPECIFICITY. THE COMBINED PERFORMANCE METRICS, IN PARTICULAR APR,  $F_2$  AND DSC INDICATE THAT THE BEST PERFORMANCE WAS ACHIEVED AT  $\beta = 0.7$ .

		3D U-Net				
Penalties		DSC	Sensitivity	Specificity	$F_2$ score	APR score
$\alpha = 0.5$ , $\beta = 0.5$		53.42	49.85	<b>99.93</b>	51.77	52.57
$\alpha = 0.4$ , $\beta = 0.6$		54.57	55.85	99.91	55.47	54.34
$\alpha = 0.3$ , $\beta = 0.7$		<b>56.42</b>	56.85	99.93	<b>57.32</b>	<b>56.04</b>
$\alpha = 0.2$ , $\beta = 0.8$		48.57	61.00	99.89	54.53	53.31
$\alpha = 0.1$ , $\beta = 0.9$		46.42	<b>65.57</b>	99.87	56.11	51.65
		3D patch-wise DenseNet + Tiling				
Penalties		DSC	Sensitivity	Specificity	$F_2$ score	APR score
$\alpha = 0.5$ , $\beta = 0.5$		67.53	68.55	<b>99.95</b>	66.02	70.5
$\alpha = 0.3$ , $\beta = 0.7$		<b>68.18</b>	74.1	99.93	<b>68.5</b>	<b>71.86</b>
$\alpha = 0.1$ , $\beta = 0.9$		62.55	<b>75.98</b>	99.91	67.03	67.75
		3D patch-wise DenseNet + Uniform Fusion				
Penalties		DSC	Sensitivity	Specificity	$F_2$ score	APR score
$\alpha = 0.5$ , $\beta = 0.5$		68.81	75.28	<b>99.94</b>	69.91	72.15
$\alpha = 0.3$ , $\beta = 0.7$		<b>68.99</b>	79.97	99.90	<b>71.96</b>	<b>73.08</b>
$\alpha = 0.1$ , $\beta = 0.9$		63.05	<b>83.55</b>	99.89	70.65	69.85
		3D patch-wise DenseNet + Spline Fusion				
Penalties		DSC	Sensitivity	Specificity	$F_2$ score	APR score
$\alpha = 0.5$ , $\beta = 0.5$		<b>70.3</b>	74.49	<b>99.95</b>	70.45	73.3
$\alpha = 0.3$ , $\beta = 0.7$		69.8	78.58	99.92	<b>71.6</b>	<b>73.59</b>
$\alpha = 0.1$ , $\beta = 0.9$		64.34	<b>81.02</b>	99.91	70.58	70.13

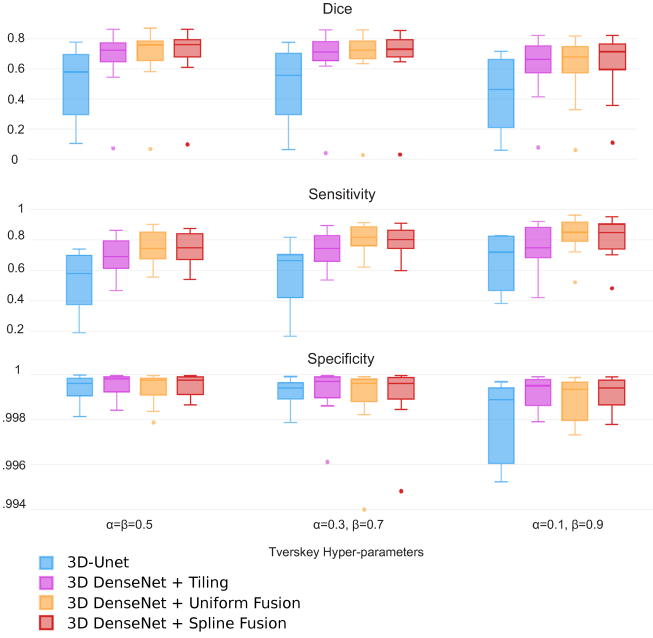


Figure 6. Boxplots of the evaluation scores: Dice, sensitivity, and specificity for the four examined approaches. Dots represent outliers outside 1.5 times the interquartile range of the upper and lower quartiles. Overall, these results show that our DenseNet model with Tversky loss function and spline patch fusion made the best trade-off between sensitivity and specificity and generated the highest Dice coefficients among all methods.

function was deliberately designed to weigh recall higher than precision (at  $\beta = 0.7$ ), consistent improvements in all test performance metrics including DSC and  $F_2$  scores on the test set indicate improved generalization through this type of training. Compared to DSC which weighs recall and precision

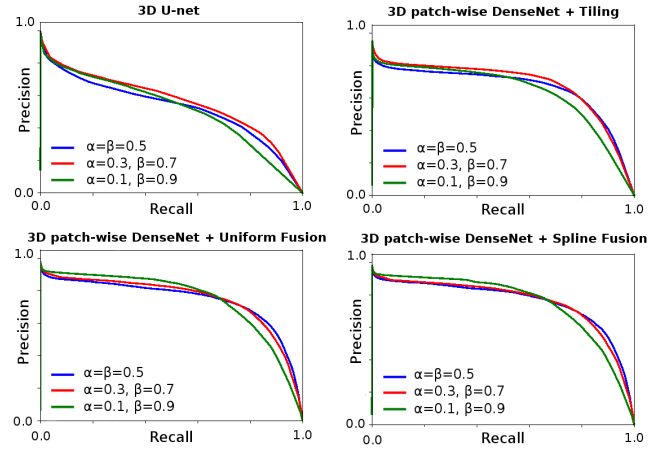


Figure 7. PR curves with different  $\alpha$  and  $\beta$  for all test set obtained by the four examined approaches. The best results based on the precision-recall trade-off were always obtained at  $\beta = 0.7$  and not with the Dice loss function.

equally, and the ROC analysis, we consider the area under the PR curves (APR, shown in Figure 7) the most reliable performance metric for such highly skewed data [40], [38].

## VI. CONCLUSION

We introduced a new loss function based on the Tversky index, that generalizes the Dice coefficient and  $F_\beta$  scores, to achieve improved trade-off between precision and recall in segmenting highly unbalanced data via deep learning. To this end, we added our proposed loss layer to two state-of-the-art 3D fully convolutional deep neural networks based on the DenseNet [29], [33] and U-net architectures [15], [9]. To put

the work in context, we reported average DSC,  $F_2$ , and APR scores of 69.8, 71.6, and 73.59, respectively, which indicate that our approach performed better than the latest methods applied in MS lesion segmentation [36], [17], [41], [42].

## REFERENCES

- [1] T. Brosch, Y. Yoo, L. Y. Tang, D. K. Li, A. Traboulsee, and R. Tam, “Deep convolutional encoder networks for multiple sclerosis lesion segmentation,” in *International Conference on Medical Image Computing and Computer-Assisted Intervention*. Springer, 2015, pp. 3–11.
- [2] K. Kamnitsas, C. Ledig, V. Newcombe, J. Simpson, A. Kane, D. Menon, D. Rueckert, and B. Glocker, “Efficient multi-scale 3D CNN with fully connected CRF for accurate brain lesion segmentation,” *Medical Image Analysis*, vol. 36, pp. 61–78, 2017.
- [3] M. Havaei, A. Davy, D. Warde-Farley, A. Biard, A. Courville, Y. Bengio, C. Pal, P.-M. Jodoin, and H. Larochelle, “Brain tumor segmentation with deep neural networks,” *Medical image analysis*, vol. 35, pp. 18–31, 2017.
- [4] S. Pereira, A. Pinto, V. Alves, and C. A. Silva, “Brain tumor segmentation using convolutional neural networks in MRI images,” *IEEE transactions on medical imaging*, vol. 35, no. 5, pp. 1240–1251, 2016.
- [5] C. Wachinger, M. Reuter, and T. Klein, “DeepNAT: Deep convolutional neural network for segmenting neuroanatomy,” *NeuroImage*, 2017.
- [6] P. Moeskops, M. A. Viergever, A. M. Mendrik, L. S. de Vries, M. J. Benders, and I. Isgum, “Automatic segmentation of MR brain images with a convolutional neural network,” *IEEE transactions on medical imaging*, vol. 35, no. 5, pp. 1252–1261, 2016.
- [7] W. Zhang, R. Li, H. Deng, L. Wang, W. Lin, S. Ji, and D. Shen, “Deep convolutional neural networks for multi-modality isointense infant brain image segmentation,” *NeuroImage*, vol. 108, pp. 214–224, 2015.
- [8] H. Chen, Q. Dou, L. Yu, J. Qin, and P.-A. Heng, “VoxResNet: Deep voxelwise residual networks for brain segmentation from 3D MR images,” *NeuroImage*, 2017.
- [9] S. S. M. Salehi, D. Erdogmus, and A. Gholipour, “Auto-context convolutional neural network (Auto-Net) for brain extraction in magnetic resonance imaging,” *IEEE Transactions on Medical Imaging*, 2017.
- [10] Ö. Çiçek, A. Abdulkadir, S. S. Lienkamp, T. Brox, and O. Ronneberger, “3D U-Net: learning dense volumetric segmentation from sparse annotation,” in *International Conference on Medical Image Computing and Computer-Assisted Intervention*. Springer, 2016, pp. 424–432.
- [11] F. Milletari, N. Navab, and S.-A. Ahmadi, “V-net: Fully convolutional neural networks for volumetric medical image segmentation,” in *3D Vision (3DV), 2016 Fourth International Conference on*. IEEE, 2016, pp. 565–571.
- [12] L. Steinman, “Multiple sclerosis: A coordinated immunological attack against myelin in the central nervous system,” *Cell*, vol. 85, no. 3, pp. 299–302, 1996.
- [13] L. A. Rolak, “Multiple sclerosis: It’s not the disease you thought it was,” *Clinical Medicine and Research*, vol. 1, no. 1, pp. 57–60, 2003.
- [14] M. Lai, “Deep learning for medical image segmentation,” *arXiv:1505.02000*, 2015.
- [15] O. Ronneberger, P. Fischer, and T. Brox, “U-net: Convolutional networks for biomedical image segmentation,” in *International Conference on Medical Image Computing and Computer-Assisted Intervention*. Springer, 2015, pp. 234–241.
- [16] A. Tversky, “Features of similarity,” *Psychological review*, vol. 84, no. 4, p. 327, 1977.
- [17] S. Valverde, M. Cabezas, E. Roura, S. González-Villà, D. Pareto, J. C. Vilanova, L. Ramió-Torrentà, A. Rovira, A. Oliver, and X. Lladó, “Improving automated multiple sclerosis lesion segmentation with a cascaded 3D convolutional neural network approach,” *NeuroImage*, vol. 155, pp. 159–168, 2017.
- [18] P. F. Christ, F. Ettlinger, F. Grun, M. E. A. Elshaer, J. Lipkov, S. Schlecht, F. Ahmady, S. Tatavarty, M. Bickel, P. Bilic, M. Rempfler, F. Hofmann, M. D’Anastasi, S.-A. Ahmadi, G. Kaassis, J. Holch, W. Sommer, R. Braren, V. Heinemann, and B. Menze, “Automatic liver and tumor segmentation of ct and mri volumes using cascaded fully convolutional neural networks,” *International Conference on Medical Image Computing and Computer Assisted Intervention*, 2016.
- [19] T. Brosch, L. Y. Tang, Y. Yoo, D. K. Li, A. Traboulsee, and R. Tam, “Deep 3d convolutional encoder networks with shortcuts for multiscale feature integration applied to multiple sclerosis lesion segmentation,” *IEEE Transactions on Medical Imaging*, vol. 35, no. 5, pp. 1–1, 2016.
- [20] M. Havaei, N. Guizard, N. Chapados, and Y. Bengio, “Hemis: Heteromodal image segmentation,” Springer, pp. 469—47, 2016.
- [21] E. Geremia, O. Clatz, B. H. Menze, E. Konukoglu, A. Criminisi, and N. Ayache, “Spatial decision forests for ms lesion segmentation in multi-channel magnetic resonance images,” *NeuroImage*, vol. 57, no. 2, pp. 378–390, 2011.
- [22] A. Jesson and T. Arbel, “Hierarchical mrf and random forest segmentation of ms lesions and healthy tissues in brain mri,” in *Proceedings of the 2015 Longitudinal Multiple Sclerosis Lesion Segmentation Challenge*, 2015, pp. 1–2.
- [23] N. Guizard, P. Coupé, V. S. Fonov, J. V. Manjón, D. L. Arnold, and D. L. Collins, “Rotation-invariant multi-contrast non-local means for ms lesion segmentation,” *NeuroImage*, vol. 8, pp. 376–389, 2015.
- [24] M. J. Fartaria, A. Roche, A. Sorega, K. O’Brien, G. Krueger, B. Maréchal, P. Sati, D. S. Reich, T. Kober, M. B. Cuadra, and C. Granziera, “Automated detection of white matter and cortical lesions in early stages of multiple sclerosis,” *Journal of Magnetic Resonance Imaging*, vol. 43, pp. 1445–1454, 2016.
- [25] X. Tomas-Fernandez and S. K. Warfield, “A model of population and subject (mops) intensities with application to multiple sclerosis lesion segmentation,” *IEEE transactions on medical imaging*, vol. 34, no. 6, pp. 1349–1361, 2015.
- [26] C. H. Sudre, W. Li, T. Vercauteren, S. Ourselin, and M. J. Cardoso, “Generalised dice overlap as a deep learning loss function for highly unbalanced segmentations,” *arXiv:1707.03237*, 2017.
- [27] X. Li, H. Chen, X. Qi, Q. Dou, C.-W. Fu, and P.-A. Heng, “A model of population and subject (mops) intensities with application to multiple sclerosis lesion segmentation,” *arXiv:1709.07330v2*, 2017.
- [28] S. S. M. Salehi, S. R. Hashemi, C. Velasco-Annis, A. Ouadlam, J. A. Estroff, D. Erdogmus, S. K. Warfield, and A. Gholipour, “Real-time automatic fetal brain extraction in fetal mri by deep learning,” *IEEE International Symposium on Biomedical Imaging*, 2018.
- [29] G. Huang, Z. Liu, L. van der Maaten, and K. Q. Weinberger, “Densely connected convolutional networks,” *Proceedings of the IEEE Conference on Computer Vision and Pattern Recognition*, 2017.
- [30] S. S. M. Salehi, D. Erdogmus, and A. Gholipour, “Tversky loss function for image segmentation using 3d fully convolutional deep networks,” *International Workshop on Machine Learning in Medical Imaging*, 2017.
- [31] J. Long, E. Shelhamer, and T. Darrell, “Fully convolutional networks for semantic segmentation,” in *Proceedings of the IEEE Conference on Computer Vision and Pattern Recognition*, 2015, pp. 3431–3440.
- [32] E. Shelhamer, J. Long, and T. Darrell, “Fully convolutional networks for semantic segmentation,” *IEEE transactions on pattern analysis and machine intelligence*, vol. 39, no. 4, pp. 640–651, 2017.
- [33] T. D. Bui, J. Shin, and T. Moon, “3d densely convolution networks for volumetric segmentation,” *arXiv:1709.03199v5*, 2017.
- [34] P. Sermanet, D. Eigen, X. Zhang, M. Mathieu, R. Fergus, and Y. LeCun, “Overfeat: Integrated recognition, localization and detection using convolutional networks,” *arXiv preprint arXiv:1312.6229*, 2013.
- [35] J. Bernal, K. Kushibar, M. Cabezas, S. Valverde, A. Oliver, and X. Lladó, “Quantitative analysis of patch-based fully convolutional neural networks for tissue segmentation on brain magnetic resonance imaging,” *arXiv preprint arXiv:1801.06457*, 2018.
- [36] O. Commowick, F. Cervenansky, and R. Ameli, “MSSEG challenge proceedings: Multiple sclerosis lesions segmentation challenge using a data management and processing infrastructure,” 2016.
- [37] D. Kingma and J. Ba, “Adam: A method for stochastic optimization,” *arXiv preprint arXiv:1412.6980*, 2014.
- [38] K. Boyd, K. H. Eng, and C. D. Page, “Area under the precision-recall curve: Point estimates and confidence intervals,” in *Joint European Conference on Machine Learning and Knowledge Discovery in Databases*. Springer, 2013, pp. 451–466.
- [39] J. Davis and M. Goadrich, “The relationship between precision-recall and ROC curves,” in *Proceedings of the 23rd international conference on Machine learning*. ACM, 2006, pp. 233–240.
- [40] T. Fawcett, “An introduction to ROC analysis,” *Pattern recognition letters*, vol. 27, no. 8, pp. 861–874, 2006.
- [41] R. McKinley, T. Gundersen, F. Wagner, A. Chan, R. Wiest, and M. Reyes, “Nabla-net: a deep dag-like convolutional architecture for biomedical image segmentation: application to white-matter lesion segmentation in multiple sclerosis,” *MSSEG Challenge Proceedings: Multiple Sclerosis Lesions Segmentation Challenge Using a Data Management and Processing Infrastructure*, pp. 46–52, 2016.
- [42] F. Vera-Olmos, H. Melero, and N. Malpica, “Random forest for multiple sclerosis lesion segmentation,” *MSSEG Challenge Proceedings: Multiple Sclerosis Lesions Segmentation Challenge Using a Data Management and Processing Infrastructure*, pp. 90–95, 2016.